Cancer Cell
Article

Enzymatic Targeting of the Stroma Ablates Physical Barriers to Treatment of Pancreatic Ductal Adenocarcinoma

Paolo P. Provenzano,[1] Carlos Cuevas,[4] Amy E. Chang,[1] Vikas K. Goel,[1] Daniel D. Von Hoff,[5] and Sunil R. Hingorani[1,2,3,*]
[1]Clinical Research Division
[2]Public Health Sciences Division
Fred Hutchinson Cancer Research Center, Seattle, WA 98109, USA
[3]Division of Medical Oncology, University of Washington School of Medicine, Seattle, WA 98195, USA
[4]Department of Radiology, University of Washington, Seattle, WA 98195, USA
[5]Clinical Translational Research Division, Translational Genomics Research Institute, Scottsdale, AZ 85259, USA
*Correspondence: srh@fhcrc.org
DOI 10.1016/j.ccr.2012.01.007

SUMMARY

Pancreatic ductal adenocarcinomas (PDAs) are characterized by a robust fibroinflammatory response. We show here that this desmoplastic reaction generates inordinately high interstitial fluid pressures (IFPs), exceeding those previously measured or theorized for solid tumors, and induces vascular collapse, while presenting substantial barriers to perfusion, diffusion, and convection of small molecule therapeutics. We identify hyaluronan, or hyaluronic acid (HA), as the primary matrix determinant of these barriers and show that systemic administration of an enzymatic agent can ablate stromal HA from autochthonous murine PDA, normalize IFP, and re-expand the microvasculature. In combination with the standard chemotherapeutic, gemcitabine, the treatment permanently remodels the tumor microenvironment and consistently achieves objective tumor responses, resulting in a near doubling of overall survival.

INTRODUCTION

Pancreatic ductal adenocarcinoma (PDA) is the fourth leading cause of cancer-related deaths in the United States (Jemal et al., 2010). The inherent biology of the disease makes it not only uniformly but also rapidly lethal: overall 5-year survival for PDA is less than 5%, with a median survival of 4–6 months (Hidalgo, 2010). Gemcitabine, a deoxycytosine analog, represents the current standard of care for advanced disease and improves quality of life in a minority of patients while prolonging survival by several weeks (Burris et al., 1997). A recent advance involving targeted inhibition of epidermal growth factor receptor (EGFR) with erlotinib extends median survival by an additional 14 days (Moore et al., 2007). Moreover, despite notable advances in surgical technique and postoperative care, and the use of adjuvant chemical and radiotherapies, virtually all early-stage patients who undergo resection also eventually succumb to recurrent and/or metastatic disease (Allison et al., 1998; Farnell et al., 2005; Oettle et al., 2007). Understanding the unusual resistance of pancreas cancer and finding ways to treat it at all stages of disease are clear and imperative needs.

Most preclinical drug evaluations to date have relied on in vitro assays and in vivo cell transplantation models. However, tumor cells arising in situ in the native organ are categorically distinct from the same cells grown in culture or engrafted into an immunocompromised mouse (Bissell and Radisky, 2001). Indeed, transplanted pancreas carcinoma cells respond readily to conventional chemotherapeutic agents (Hertel et al., 1990), in marked contrast to autochthonous tumors in mice (Olive et al., 2009) and humans (Tempero et al., 2003). This problem cuts both ways: in failing to fully appreciate the unique challenges imposed by the complex cancer "organ," opportunities to target

Significance

More than 90% of cancer drugs brought to the clinic fail. The gap between preclinical promise and clinical reality arises, in part, from the inability of traditional model systems to sufficiently represent the cellular and structural complexity of the solid tumor "organ." In failing to fully account for the tremendous obstacles to efficacy in autochthonous tumors, potential opportunities to identify and target the most clinically meaningful barriers are also lost. We have found that an unusually abundant matrix glycosaminoglycan fortifies the epithelium and creates a drug-free sanctuary in PDA. Ablating this constituent renders the cancer profoundly vulnerable to standard cytotoxics and holds promise as a distinct therapeutic strategy, while compelling reassessment of conventional chemotherapies previously thought to be ineffective.

and exploit the most clinically relevant mechanisms may also be missed. Thus, there are noncell autonomous factors, including unique cell-cell and cell-matrix interactions and evolving intratumoral physical dynamics, that contribute to the in vivo resistance of cancers.

Prior work in a number of experimental systems has suggested that altered intratumoral fluid dynamics can limit the effectiveness of systemic therapies (reviewed in Bouzin and Feron, 2007; Heldin et al., 2004; Jain, 1987; Trédan et al., 2007). Mammalian organs and tissues typically possess interstitial fluid pressures (IFPs) at or below the intravascular pressures (IVPs) in the terminal arterioles and capillaries that supply them. As first proposed by Starling in 1896, an IFP less than IVP permits ready perfusion and favors diffusive and convective forces necessary for solute and fluid flow into the interstitium (Starling, 1896; see Supplemental Information available online). The solutes are consumed by cells, while the venous vasculature and functional lymphatic channels return excess fluid to the systemic circulation (reviewed in Michel, 1984). Although these processes governing the delivery and diffusion of cancer drugs have been studied extensively in xenograft models, very few experiments have been performed in autochthonous carcinomas, and no rigorous analyses before and after perturbation of the tumor microenvironment have been described.

PDAs are characterized by an unusually intense desmoplastic reaction composed of fibroblasts, immune cells, and endothelial cells embedded within a dense and complex extracellular matrix (ECM). The ECM component hyaluronic acid (HA), or hyaluronan, is inordinately abundant, inviting speculation on its role in disease biology and resistance. HA is a large linear glycosaminoglycan (GAG), composed of repeating N-acetyl glucosamine and glucuronic acid units, and figures prominently in the architecture, integrity, and malleability of tissues, particularly in dynamic processes such as embryogenesis and oncogenesis (Toole, 2004). Its viscoelastic properties underlie its unique role in tissue homeostasis and its appeal in cosmetic and clinical applications (Balazs and Denlinger, 1989). HA also communicates directly with cells in health and disease through interactions with several distinct types of surface receptors. However, the abundance of HA varies widely across tumors, and it has been shown to both promote and suppress tumor growth (Toole, 2004). Even its potential contribution to IFP is controversial. Local injection of hyaluronidase into osteosarcoma xenografts has been shown to decrease IFP (Brekken et al., 2000; Eikenes et al., 2005), although enforced overexpression of HA in thyroid and colon carcinoma xenografts did not increase it (Jacobson et al., 2003). Thus, although HA has been implicated in a variety of cell autonomous and noncell autonomous processes, its precise role(s) in therapeutic resistance of cancers has remained elusive and is likely context specific (reviewed in Toole and Slomiany, 2008; Trédan et al., 2007).

As an alternative to transplanted cells and tumors, we have developed genetically engineered mouse (GEM) models of PDA that faithfully recapitulate the clinical syndrome, histopathology, and molecular progression of human pancreas cancer from inception to invasion. *Kras*$^{LSL\text{-}G12D/+}$*;Cre* (*KC*) (Hingorani et al., 2003) and *Kras*$^{LSL\text{-}G12D/+}$*;Trp53*$^{LSL\text{-}R172H/+}$*;Cre* (*KPC*) (Hingorani et al., 2005) mice conditionally express endogenous, physiologic levels of the respective oncogene and tumor suppressor gene mutations in pancreatic progenitor cells, resulting in the stochastic development and spontaneous progression of preinvasive ductal lesions to invasive and metastatic carcinomas. In collaborative studies using the *KPC* model, we have recently suggested that the unusually hypovascular microenvironment of PDA compromises the delivery of even small molecule therapeutics such as gemcitabine. These studies showed further that targeting stromal fibroblasts by disrupting paracrine Hedgehog signaling between the epithelial and mesenchymal tumor compartments transiently increased the apparent microvascular density through neoangiogenesis and improved drug delivery, resulting in a modest survival benefit (Olive et al., 2009). Interestingly, disease resistance rapidly re-emerged along with a return of the profound hypovascularity. Moreover, the mechanisms giving rise to and sustaining this paucity of vessels remained unclear. In the present study, we pursue a mechanistic understanding of the biophysical barriers to perfusion, diffusion, and convection imposed by the desmoplastic reaction in autochthonous PDA and investigate strategies to surmount them.

RESULTS

Cellular and Molecular Evolution of Desmoplasia in PDA

As part of a systematic effort to characterize the evolving stromal dynamics and potential therapeutic vulnerabilities during disease progression, we performed specific histochemical and immunohistochemical assays to identify components of the ECM and infiltrating cells in preinvasive, invasive, and metastatic PDA in mice and humans (Figure 1 and Figures S1A–S1D). A robust and definable stromal reaction develops in association with early precursor lesions and includes a dense collagen content organized in a fibrillary structure in both primary tumors and metastases, as revealed by intravital second harmonic generation (SHG) imaging (Figures S1E–S1J). The tight association of this fibrillar collagen with epithelial carcinoma cells became evident in *Kras*$^{LSL\text{-}G12D/+}$*;Trp53*$^{LSL\text{-}R172H/+}$*;R26*$^{LSL\text{-}GFP/+}$*;Cre* (*KPGC*) mice. Interestingly, the relative concentrations of collagen and glycosaminoglycans (GAGs) appear to alter during disease progression, shifting toward higher GAG content at more advanced and metastatic stages of disease (Figures 1A–1J). One particular GAG, HA, was especially abundant (Figures 1K–1O), which was confirmed by treating tissue sections with hyaluronidase (Figures S1K–S1N). We note that significant HA deposition begins with early precursor lesions (Figures 1G and 1L). In addition, activated stromal pancreatic stellate cells (PSCs), or myofibroblasts, also infiltrate early and are prevalent throughout disease progression (Figures 1P–1T). Conversely, a decrease in vessel number is seen with progression (Figures S1O–S1Q), as described previously (Olive et al., 2009), and is accompanied by a decrease in cross-sectional (luminal) area (Figure S1R).

This same overall molecular and cellular stromal composition is observed in human PDA (Figures 1E, 1J, 1O, and 1T). We note, in particular, the expression of moderate-to-high levels of HA in all human PDAs tested (n = 30; Figures 1J and 1O and data not shown), suggesting that this substrate may be an essential component of disease architecture, biology, and resistance.

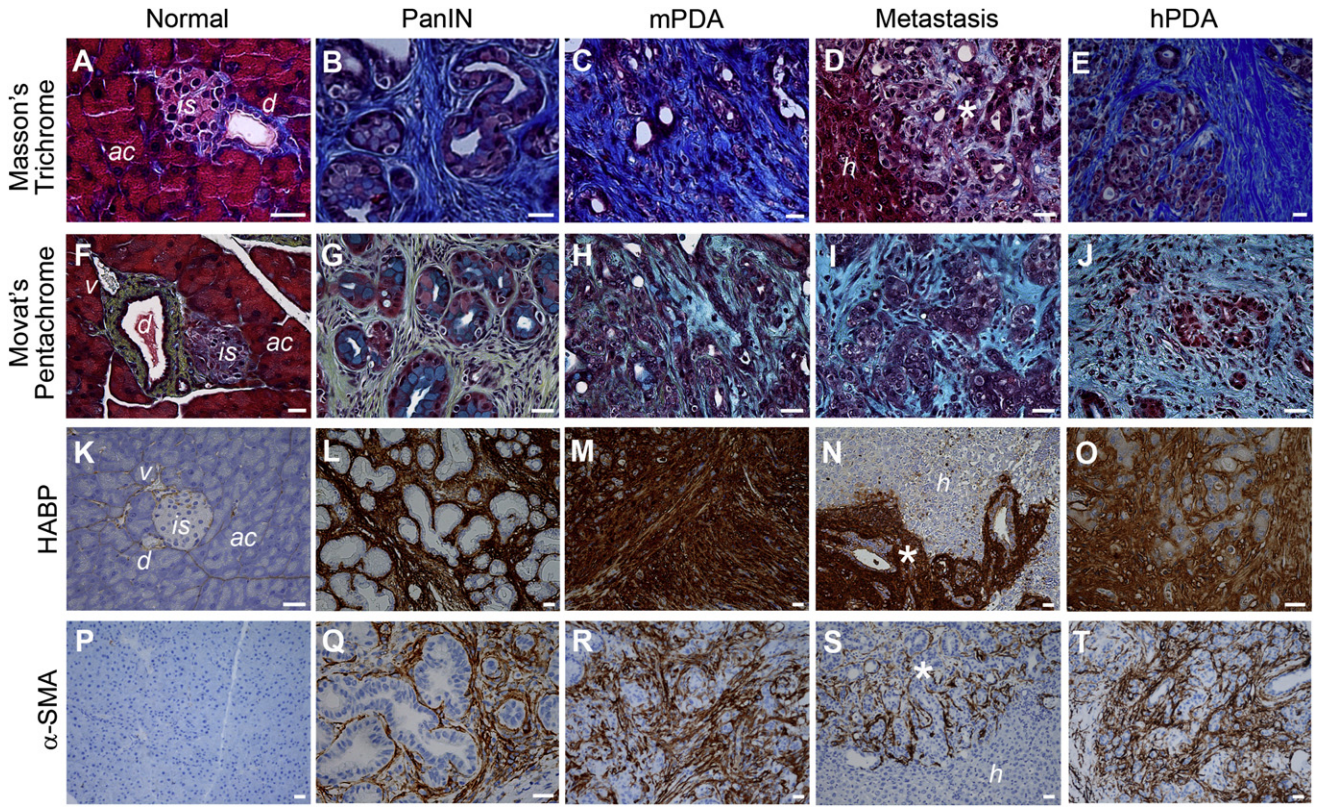

Figure 1. Evolution of the Desmoplastic Reaction in Murine and Human PDA

(A–E) Masson's trichrome histochemistry shows robust collagen deposition (blue) at all stages of disease.

(F–J) Movat's pentachrome histochemistry reveals collagen (yellow), GAGs and mucins (blue), and their colocalization (turquoise/green).

(K–O) Histochemistry with HA-binding protein (HABP) reveals intense HA content beginning with preinvasive disease (PanIN).

(P–T) Activated PSC express α-smooth muscle actin (α-SMA) and are abundant in preinvasive (Q), invasive (R) and metastatic mPDA (S) and hPDA (T), but not in normal pancreata (P). *ac,* acini; *is,* islet; *d,* duct; *v*, venule; *h*, hepatic parenchyma; *, metastatic lesions. Scale bars, 25 μm. See also Figure S1.

Dramatically Elevated IFP in PDA

To directly measure IFP in normal pancreata and in autochthonous PDAs in live animals, we used a system coupling a miniature piezoelectric pressure transducer to a pressure control unit and data acquisition module (Figure 2A). Anesthetized animals underwent laparotomy followed by needle-guided placement of the pressure transducer probe enabling real-time in vivo IFP measurements (Figures 2B and 2C). As expected, the normal pancreas possesses an IFP ranging between 8 and 13 mm Hg (mean = 10.4 mm Hg; n = 8) (Figure 2D). In contrast, we observed dramatically elevated IFPs in autochthonous PDA that far exceeded the normal range for the pancreas (Figure 2D). Tumor IFPs ranged from 75 to 130 mm Hg (mean = 99 mm Hg, n = 7, in *KPC* PDA; mean = 87 mm Hg, n = 4, in *KC* tumors), which vastly exceeded typical arteriolar and capillary pressures of 40–80 mm Hg and 15–40 mm Hg, respectively (Sherwood, 1997) and rivaled mean arterial pressure (Janssen et al., 2000; Mattson, 1998). Pressures of this magnitude suggest not only major impediments to delivery and convection of small molecules, but also imply a profound reorganization and remodeling of the tumor architecture and the forces operant within it (see also Supplemental Information).

Enzymatic Targeting of Stromal HA Restores Tumor IFP and Functional Perfusion

We began our studies on the ability of HA to elevate IFP using reconstituted three-dimensional matrices. Purified primary murine PDA cells were embedded in matrices with differing HA concentrations, the tumor plugs were implanted in immunodeficient mice, and IFPs were recorded (Figures S2A–S2C). HA concentrations of 3 mg/ml more than doubled the baseline IFP of carcinoma cells engrafted in collagen alone, suggesting that the presence of HA in the tumor can contribute directly to elevated IFP.

The abundance of HA in PDA and its demonstrated capacity to significantly elevate IFP prompted us to investigate whether a systemically delivered agent could ablate HA in the stroma of an autochthonous PDA and decrease pressures. We first tested the ability of intravenously administered PEGPH20 to deplete HA from normal tissues in wild-type (*WT*) mice and assessed for any untoward effects (Figures S2D–S2F). Several organs in the body including heart, lung, bowel, and liver contain modest levels of detectable HA (Figure S2E), whereas joints possess very high levels (Figure S2F). HA was efficiently ablated from all of these sites except cartilage and the surrounding joint space. Cartilage

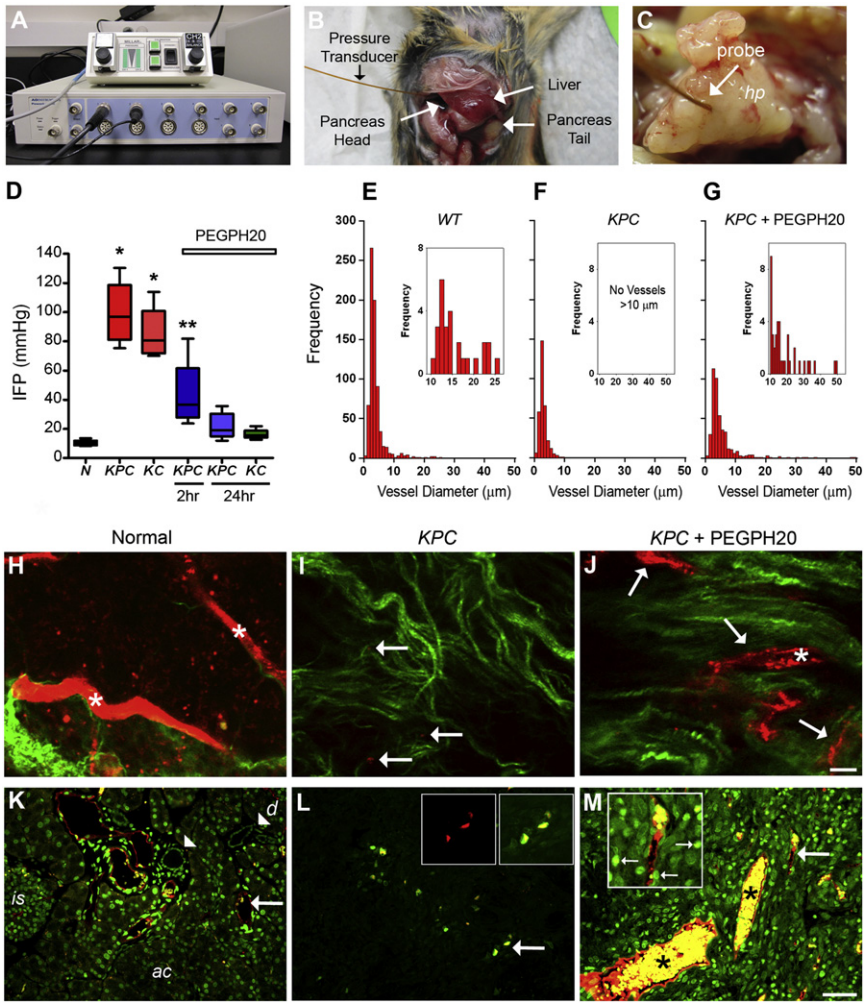

Figure 2. Elevated IFP Compromises Vascular Function in PDA

(A) Experimental apparatus to measure IFP.

(B and C) IFP probe positioned in PDA at the head of the pancreas (*hp*). In (B), the probe ends in a tumor obscured by the overlying liver.

(D) IFP measurements in normal pancreata (*N*), untreated *KPC* and *KC* tumors and tumors 2 and 24 hr after PEGPH20 treatment. *p < 0.01 for comparison between normal pancreata and PEGPH20 treatment groups; **p < 0.05 for difference from all other groups with 1-way ANOVA and Newman-Keuls posthoc multiple comparison test. Note that IFP levels in normal pancreata and PEGPH20-treated *KC* (mean = 16 mm Hg, n = 4) and *KPC* (mean = 22 mm Hg, n = 5) tumors 24 hr after treatment were not statistically different. Box and whisker plots: boxes display the lower (25^{th}) and upper (75^{th}) quartiles with a line at the median; whiskers extend from the minimum to the maximum observation.

(E–G) Distribution of $CD31^+$ vessel diameter in normal pancreata (E), untreated *KPC* tumors (F), and *KPC* tumors 24 hr after PEGPH20 treatment (G). Insets show data for vessels of diameter > 10 μm. Data represent evaluations from four independent sections from each of four separate animals for each condition and are significantly different ($p < 0.0001$) in the pairwise comparisons with *KPC*.

(H–J) Multiphoton excitation of fluorescently conjugated lectin (red) and second harmonic generation imaging of collagen (green) within intact normal pancreas (H), untreated *KPC* tumors (I), and *KPC* tumors 24 hr after PEGPH20 treatment (J). Asterisks in (H) and (J) highlight examples of large functional vessels. Arrows in (I) and (J) indicate perfused (functional) vessels. Note that when a rare functional vessel in untreated *KPC* tumors is identified, it is extremely small relative to those in normal pancreata and PEGPH20 treated tumors. Scale bar, 10 μm for (H–J).

(K–M) Direct fluorescence analysis of Alexa-647-conjugated lectin (red) and doxorubicin (green) in intact normal pancreas (K), untreated *KPC* tumors (L), and *KPC* tumors 24 hr after PEGPH20 treatment (M). Arrow in (K) shows an example of a widely patent, thin-walled vessel, and arrowheads indicate ductal epithelium. Large arrows in (L) and (M) highlight regions magnified in respective inset boxes. The left inset box in (L) shows signal in the far-red Alexa-647 channel (lectin) alone, and the right inset box shows merged green (doxorubicin) and red (lectin) channels. Small arrows in inset box of panel (M) identify examples of specific nuclear staining from DNA-bound doxorubicin, as well as the presence of free doxorubicin in the tumor. Asterisks in (M) highlight examples of large, functional lectin-positive vessels loaded with doxorubicin. *ac,* acini; *is,* islet; *d,* duct. Scale bar, 50 μm for (K–M). See also Figure S2.

represents an essentially avascular compartment completely excluding delivery of PEGPH20. Interestingly, depletion of HA from these sites had no discernible effects on organ function or animal health; animals remained active without apparent changes in energy level or mobility and also maintained their body weight (Figure S2D). We next demonstrated that intravenous administration of PEGPH20 to *KC* and *KPC* mice could deplete HA in autochthonous PDAs (Figure S2G). Moreover, after a single intravenous dose of PEGPH20, IFP was significantly decreased within 2 hr and approached the range for normal pancreata 24 hr after treatment (Figure 2D). The restoration of near normal tumor IFP after degradation of stromal HA suggested that treatment with PEGPH20 should also significantly and rapidly improve blood flow if indeed mechanical compression of the vasculature was the primary mechanism limiting perfusion. To assess the effects on the tumor microvasculature of IFP normalization, we performed a systematic survey of vessel number and lumen diameter in WT pancreata as well as untreated and treated murine PDA (Figures 2E–2G). We found a significant shift in the distribution of $CD31^+$ vessel diameters in murine and human PDA compared with the normal pancreas and, in particular, an almost complete absence of large diameter (>10 μm) vessels (Figures 2E–2G and Figures S2H and S2I). The normal pancreas contains a range of small-to-moderate sized vessels, more than 80% of which possess a readily discernible and patent lumen; conversely, the majority (~75%) of vessels in PDA lacked an apparent lumen, consistent with vascular collapse from elevated extrinsic fluid pressures. Following treatment with PEGPH20, vessel diameter was significantly increased and lumens clearly discernible in ~71% of $CD31^+$ vessels (Figure 2G and Figure S2H).

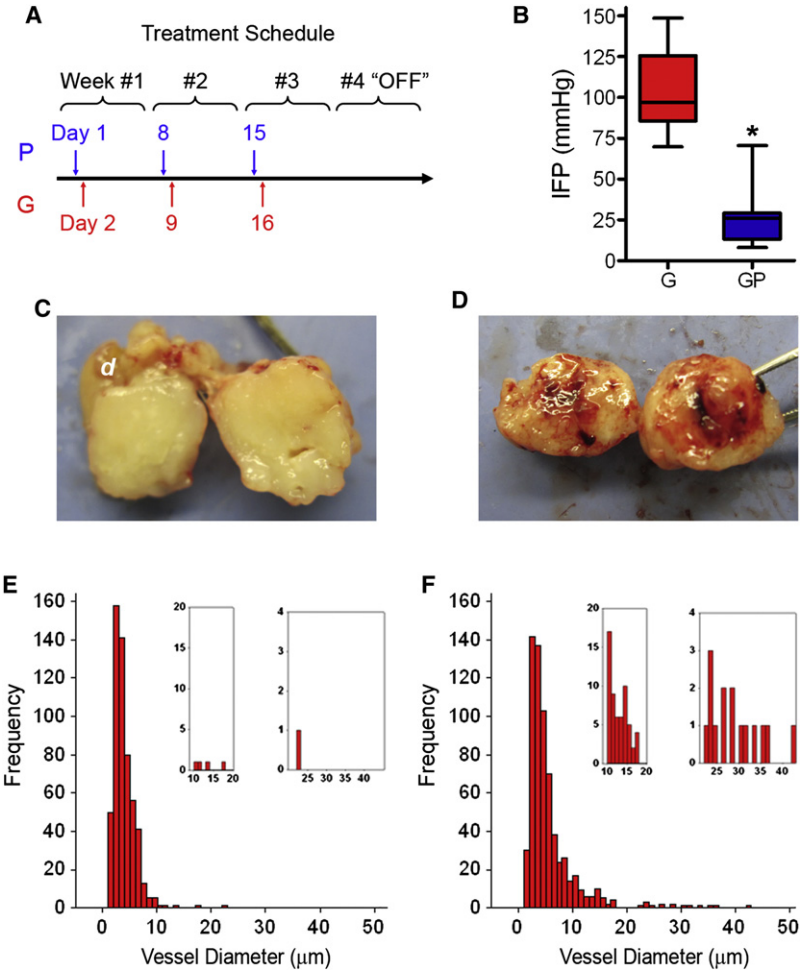

Figure 3. Gemcitabine+PEGPH20 Combination Therapy Fundamentally Changes the Tumor Vasculature

(A) Treatment schedule for administration of PEGPH20 (P) or placebo and gemcitabine (G). Mice undergoing gemcitabine monotherapy also received placebo (vehicle) injections. Each 4-week course represents one cycle of therapy.

(B) Tumor IFP at survival endpoint after treatment with gemcitabine (G; n = 9) or Gem+PEGPH20 (GP; n = 9), *p < 0.0001. Box and whisker plots: boxes display the lower (25th) and upper (75th) quartiles with a line at the median; whiskers extend from the minimum to the maximum observation.

(C) Gross pathology of transected PDA at endpoint after gemcitabine monotherapy. *d*, duodenum.

(D) Gross pathology of transected PDA at endpoint after combination therapy.

(E and F) Distribution of significantly different ($p < 0.0001$) CD31$^+$ vessel diameter in Gem (E) and Gem+PEGPH20 (F) treated *KPC* tumors at survival endpoint. Inset graphs show significantly different ($p < 0.0001$) distribution also for subsets of vessels with diameters between 10–20 μm and > 20 μm. Data are from four independent sections from five separate animals for each treatment arm. See also Figure S3.

We next performed functional analyses of the vasculature with intravital multiphoton laser scanning microscopy (MPLSM). Normal pancreata revealed a rich, widely patent vasculature (Figure 2H) with excellent delivery of the small molecule therapeutic doxorubicin throughout the parenchyma (Figure 2K). In contrast, vessels in PDA were difficult to detect and appeared collapsed (Figure 2I), and penetration of doxorubicin into the tumor bed was extremely limited (Figure 2L). Even when rare perfusion was observed (Figure 2L), the distribution of drug into the tumor was low, suggesting limited diffusion and convection into the interstitium. A single intravenous dose of PEGPH20 resulted in the immediate appearance of significant numbers of patent vessels (Figures 2J and 2M), reflecting their increased diameters (Figure 2G). These changes were accompanied by a >6.5-fold increase in doxorubicin fluorescence intensity over baseline ($p = 0.013$, $n = 4$ each for treated and untreated *KPC* cohorts; and $p = 0.04$, $n = 3$ per group for *KC* PDAs). We note that overall vessel number did not significantly change (data not shown), which, together with the rapidity of the effect and lack of significant endothelial cell proliferation (see below), suggest that neoangiogenesis did not contribute substantively. Rather, it appears that the inordinately high IFP produces vascular collapse in PDA and reversal of these elevated pressures restores functional perfusion and unimpeded delivery of drug into the carcinoma.

Combined Enzymatic and Cytotoxic Chemotherapy Alters Tumor Biology and Increases Disease Response and Overall Survival in PDA

We next sought to assess the effects of combination chemotherapy on the gross morphological, physicomechanical, cellular, and molecular properties of autochthonous PDA. In previous studies of gemcitabine in *KPC* mice (Olive et al., 2009), we used a dose, route, and schedule modeled on the original preclinical investigations of gemcitabine in subcutaneously engrafted tumors (Hertel et al., 1990; Schultz et al., 1993). For the present studies, we treated *KPC* cohorts according to the route and schedule used in the clinic. Specifically, we performed a randomized, placebo-controlled study of the combination regimen involving intravenous drug administration in cycles consisting of the 3-weeks "on" and 1-week "off" schedule used in patients (Figure 3A). Animals were first assessed with serial high-resolution ultrasound measurements until they achieved a requisite enrollment tumor diameter of 2–5 mm. Studies were performed on separate cohorts of animals to measure early and intermediate effects, and also to establish overall survival.

As expected, IFP normalized in Gem+PEGPH20-treated tumors, confirming that the addition of gemcitabine did not impede the ability of PEGPH20 to influence this physicomechanical property (Figure 3B). Interestingly, no change in baseline tumor IFP occurred in Gem+Placebo-treated animals, reflecting the inability of gemcitabine to effectively penetrate tumors and induce responses. The gross findings at necropsy underscored these differences, as tumors recovered from Gem+Placebo-treated animals (Figure 3C and Figure S3A) revealed the hard,

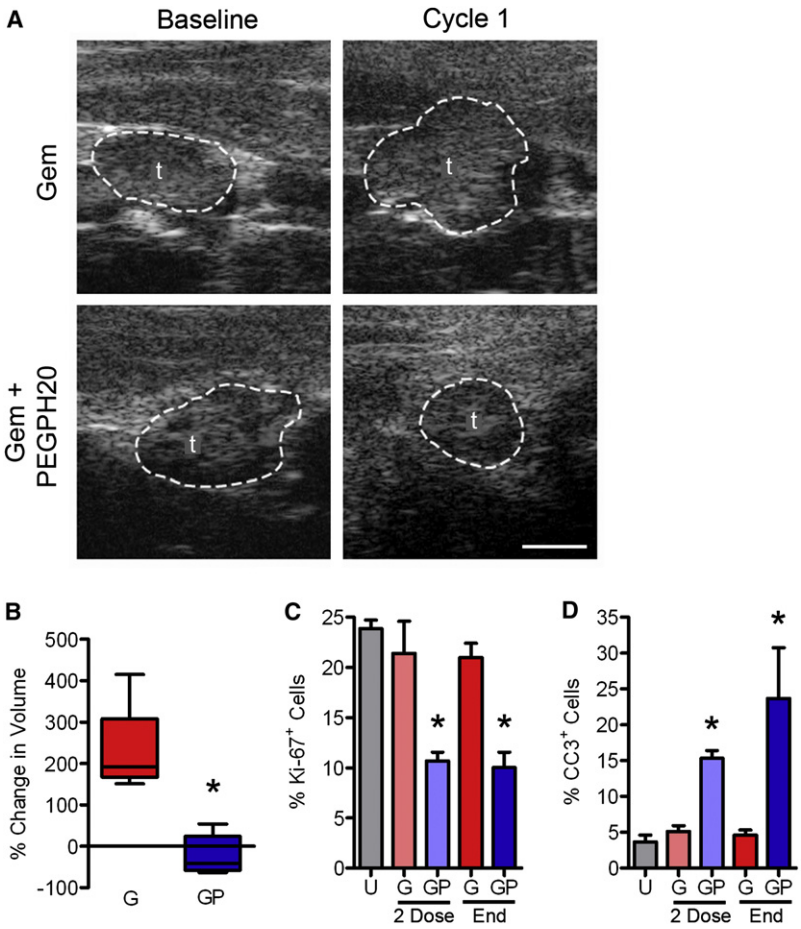

Figure 4. Gemcitabine+PEGPH20 Induces Objective Responses through Reduced Proliferation and Increased Apoptosis

(A) High-resolution ultrasound images of PDA before and after the indicated treatment. Scale bar, 1 mm. t, tumor.

(B) Quantitative analysis of tumor volume in Gem (G; n = 5) and Gem+PEGPH20 (GP; n = 6) treated mice after one cycle of therapy (*p = 0.009). Box and whisker plots: boxes display the lower (25th) and upper (75th) quartiles with a line at the median; whiskers extend from the minimum to the maximum observation.

(C) Quantitative analysis of proliferation assessed as percentage of Ki-67^{+} cells per image field in untreated (U) and Gem (G) or Gem+PEGPH20 (GP) treated tumors after either two weekly doses of therapy (2 Dose; *p < 0.035) or at endpoint (End; *p = 0.0009).

(D) Quantitative analysis of apoptosis assessed as percentage of cleaved caspase-3 (CC3)$^{+}$ cells per image field in untreated (U) and Gem (G) or Gem+PEGPH20 (GP) treated tumors after two doses of therapy (*p = 0.035) or at endpoint (*p = 0.01). Data in (C and D) are plotted as mean ± SEM. See also Figure S4.

white, fibrous, and overtly hypovascular composition typical of the untreated disease (Figure S3B). In contrast, tumors from animals receiving Gem+PEGPH20 were notably soft, highly vascularized, and even hemorrhagic when transected (Figures 3D and Figures S3C–S3F). A blood-rich microenvironment in combination treated tumors was readily apparent even by routine histology (Figures S3G–S3L). Quantitative analysis confirmed significant differences in vessel diameter between Gem+Placebo- and Gem+PEGPH20-treated PDA (Figures 3E and 3F) without significant differences in vessel number (data not shown). Importantly, these findings were observed in all mice immediately after initiating therapy (Figures S3G–S3L), during active treatment (Figures S3M and S3N), and persisted even after treatment cessation (Figures S3O–S3T). Even nearly 3 months after completing combination therapy, functional vessels were retained suggesting an irreversible change in tumor physiology (Figures S3S and S3T).

Objective measures of clinical response were frequently apparent after only one cycle of combination therapy. Notably, of the subset of Gem+Placebo-treated animals that underwent quantitative volumetric imaging both before and after treatment, none experienced an objective tumor response affirming the collective clinical (Burris et al., 1997; Casper et al., 1994) and preclinical experience with this agent in autochthonous PDA (Olive et al., 2009) (Figures 4A and 4B). In contrast, 83% of Gem+PEGPH20-treated tumors decreased in size after one cycle of treatment (Figures 4A and 4B) with all tumors responding after three cycles (see example in Figure S4A). Consistent with its known mechanisms of inhibiting DNA and RNA synthesis (Hertel et al., 1990; Ueno et al., 2007), combination therapy both decreased proliferation and increased apoptosis of primary tumor cells compared with Gem+Placebo, contributing to the observed differences in objective responses (Figures 4C and 4D and Figures S4B–S4E). Thus, when able to penetrate the tumor bed, gemcitabine can indeed be an effective agent against this disease.

The numbers of total stromal PSCs (Figure S5A) and activated PSCs (Figures 5A–5C and Figure S5B) were also significantly decreased, and the tumor stroma was extensively remodeled (Figures 5D–5G). Although unaffected by PEGPH20 alone, collagen content and distribution were both significantly decreased by the combined regimen, likely as a secondary consequence of depleting collagen-secreting activated PSCs. Finally, no discernible effects on endothelial cell proliferation (Figure S5C) or apoptosis (Figure S5D) were observed, consistent with the expected restricted activity of a conventional cytotoxic agent to actively dividing cells. Thus, the depleted HA and diminished IFP seen with the combined enzymatic and cytotoxic regimen restores and preserves a functional vasculature while inducing tumor epithelial and stromal cells to die.

Similar restrictions and responses were observed in metastases. Metastatic lesions to the liver (Figures 1D, 1I, 1N, and 1S) and lung (Figure 6A) possessed a robust and complex desmoplasia, with notable HA content and a paucity of vessels (Figures S6A–S6G). Perhaps surprisingly, given their typically smaller size compared with primary tumors, the metastatic deposits were also poorly perfused by small molecules (Figures S6H–S6K). As with primary tumors, PEGPH20 efficiently ablated HA from metastases (Figure 6B) and restored functional perfusion (Figure S6K).

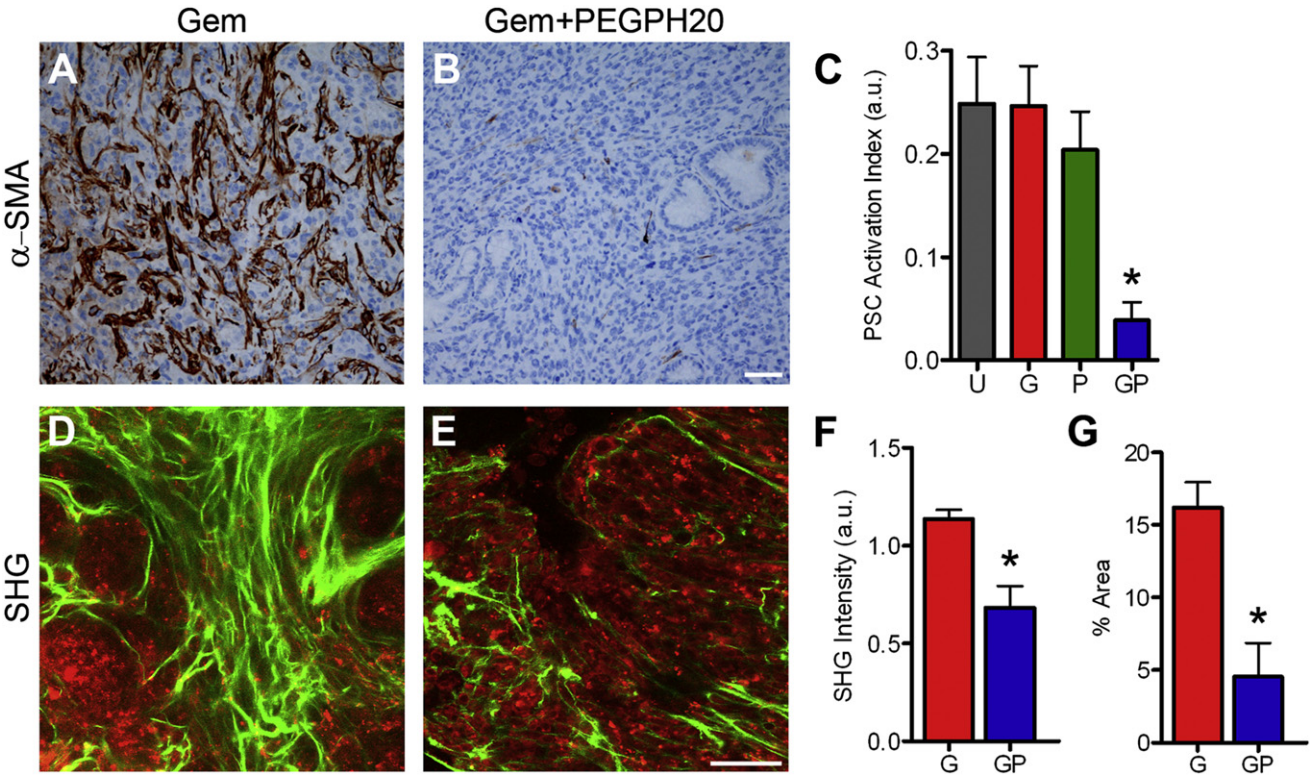

Figure 5. Combination Therapy with Gemcitabine+ PEGPH20 Remodels the Tumor Stroma

(A and B) IHC for the PSC activation marker α-SMA in PDA at survival endpoint after the indicated treatment. Scale bar, 50 μm.

(C) Quantitative analysis of PSC activation in untreated tumors (U) or tumors treated with Gem (G), PEGPH20 (P), or Gem+PEGPH20 (GP) at survival endpoint (*p = 0.005).

(D and E) Representative micrographs from intravital SHG imaging of collagen (green) combined with multiphoton excitation of endogenous fluorescence from NADH (red) in PDA at survival endpoint just prior to euthanasia. Scale bar, 50 μm.

(F) Mean SHG intensity in PDAs at endpoint as a measure of fibrillar collagen concentration (*p = 0.028).

(G) Percent area occupied by fibrillar collagen in tumors at endpoint (*p = 0.028). Data in (C), (F), and (G) are plotted as mean ± SEM. See also Figure S5.

When given together with gemcitabine, the combination regimen decreased proliferation (Figure 6C) and increased apoptosis (Figure 6D) in metastases to both distant sites.

The aforementioned encouraging results notwithstanding, the most clinically relevant measure of efficacy is survival. We therefore performed a prospective, randomized, placebo-controlled trial in *KPC* mice with overall survival as the primary endpoint. Secondary endpoints included changes in intratumoral IFP and objective response rates, as well as metastatic disease burden.

Median overall survival increased from 55.5 days for Gem+Placebo to 91.5 days for Gem+PEGPH20, an 83% increase (Figure 6E). These results likely do not reflect the maximal achievable benefit from combination therapy as the treatment course was limited to 3 months because of sclerosing of the vein after repeated intravenous injections. In fact, only 29% of Gem+PEGPH20-treated animals died during the course of therapy and approximately 30% of animals lived an additional 4–11 weeks after completing three full months of treatment. In contrast, more than 80% of animals receiving Gem+Placebo died during treatment; of the remaining four animals, three died in the very next week after cessation of therapy (Figure 6E and Table S1).

The metastatic tumor burden was also significantly diminished with combination therapy (Figure 6F, Table 1, and Table S1). The frequency of malignant ascites as well as metastases to the liver, lungs, diaphragm, and mesenteric lymph nodes were all decreased in the Gem+PEGPH20 cohort. Thus, the combination regimen effectively treated both the primary and metastatic disease burdens.

DISCUSSION

The defining features of PDA are a penchant for metastatic spread and a notorious resistance to chemical and radiotherapies. These features, in turn, establish the major hurdles to meaningful treatment of the disease. A perhaps prosaic, albeit unexpected and critically important, barrier to systemic therapy is a profoundly diminished functional vasculature in PDA. We show here that the primary mechanism limiting perfusion in PDA is significant collapse of resident vessels by inordinately high fluid pressures. Small molecules that are delivered to the tumor bed are subsequently impeded from penetrating the interstitium by constraints on diffusion and convection, completing a trifecta of stromal barriers to chemotherapy. Enzymatic

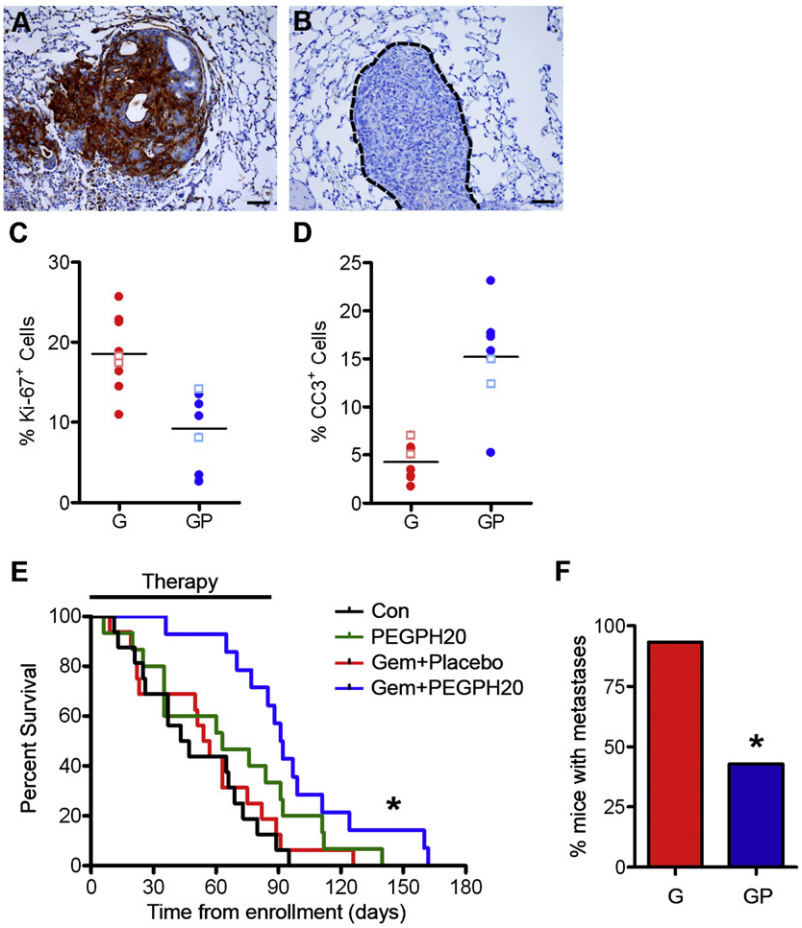

Figure 6. Gemcitabine+PEGPH20 Combination Therapy Decreases Metastatic Tumor Burden and Improves Survival

(A and B) HA expression in lung metastases from untreated (A) and PEGPH20-treated (B) animals.

(C) Quantitative analyses of proliferation assessed as percentage of Ki-67$^+$ cells in metastases to liver (filled circles) and lung (open squares) after gemcitabine monotherapy (G) or Gem+PEGPH20 (GP) combination therapy ($p = 0.0012$). Horizontal bars represent means.

(D) Quantitative analysis of apoptosis assessed as percentage of CC3$^+$ cells in liver (filled circles) and lung (open squares) metastases ($p = 0.0001$). Horizontal bars represent means.

(E) Kaplan-Meier survival curves from time of enrollment in control (Con; n = 16), Gem (n = 16), PEGPH20 (n = 15), and Gem+PEGPH20-treated *KPC* animals (n = 14). (Black bar indicates maximum duration of therapy.) Median overall survival of Gem (55.5 days) and Gem+PEGPH20 (91.5 days) treated mice are significantly different (*$p = 0.004$). Treatment with PEGPH20 alone showed a trend toward increased survival (median = 63 days) that did not reach statistical significance ($p = 0.1$).

(F) Metastatic burden in Gem+PEGPH20 (GP) treated mice is significantly decreased compared with Gem treatment alone (G) (*$p = 0.014$). See also Figure S6 and Table S1.

degradation of hyaluronan results in a rapid reduction of IFP accompanied by the appearance of widely patent functioning vessels. Removing these barriers permits high concentrations of chemotherapy to reach the tumor, resulting in improved survival and revealing an unappreciated sensitivity of the disease to conventional cytotoxic agents.

The theory governing the movement of fluid and solute across a semipermeable membrane dividing two compartments (e.g., vascular and extravascular) is readily derived from fundamental thermodynamic principles (Kedem and Katchalsky, 1958; Kedem and Katchalsky, 1961; Staverman, 1952) (reviewed in Ogston and Michel, 1978) and incorporates hydrostatic and osmotic pressure gradients as the primary determinants of fluid flow, and concentration gradients as the driving force for solute flux. The resultant equations, in turn, explain the inability to achieve effective chemotherapy concentrations in PDA given the extremely high IFPs observed (see Supplemental Information for a detailed treatment of these equations). They do not, however, adequately address how such dramatically elevated IFPs arise in the first place. The prevailing hypotheses envision the intravascular and interstitial compartments to be in contiguity or communication, suggesting that changes in IFP chronicle and directly reflect intratumoral vascular pressures largely as a consequence of "leaky" or damaged vessels (Boucher and Jain, 1992; Netti et al., 1999). However, the essentially complete collapse of the microvasculature in invasive PDA implies that this relationship no longer holds and that forces other than intravascular pressure must be maintaining the dramatically elevated IFP. Indeed, we have observed a sustained elevation of tumor IFP even after the cessation of cardiac function (unpublished observations), underscoring the disconnect between intravascular pressure and IFP in this setting. Some models also postulate an elevated interstitial permeability in tumors (Jain, 1990), which appears not to be the case in PDA and, in any event, would favor not hinder delivery of (macro)molecules. Thus, despite an extensive history of studies in experimental systems and limited work in human cancers in situ (Boucher et al., 1991; Curti et al., 1993; Less et al., 1992), the magnitude of interstitial hypertension in solid tumors has clearly been underestimated, particularly with respect to PDA, and the mechanisms driving its genesis have remained elusive.

Plausible mechanisms to further elevate interstitial pressure include an ECM production sufficiently prolific to increase tumor density more rapidly than volume, and/or robust cell contractility that actively compacts the tumor (Reed et al., 1992). In this regard, the ability of a systemically delivered enzyme to dissipate the high IFPs in PDA not only holds great therapeutic promise but also provides insight into the underlying physicomechanical processes operant within this complex cancer environment (Figure 7). Intact HA functions as a hydrated gel generating an immobile fluid phase that secondarily also diminishes compressibility (tethered collagen fibers under tension provide the primary framework for rigid structure). We propose that PEGPH20 first liberates water bound to HA through cleavage of the extended polymer into substituent units. The release of trapped water

Table 1. Summary of Metastatic Disease Burden in *KPC* Mice

Treatment	Mice with Metastatic Disease (%)	No. of Macroscopic Metastases/ Mouse (mean ± SEM)	No. of Metastases/ Mouse (mean ± SEM)	Mice with Liver Metastases (%)	Mice with Lung Metastases (%)	Mice with Diaphragm Metastases (%)	Mice with Lymph Node Involvement (%)	Mice with Malignant Ascites (%)
Gem+Placebo	93	1.7 ± 0.35	2.4 ± 0.35	73	40	40	73	47
Gem+PEGPH20	43	0.86 ± 0.4	1.1 ± 0.4	43	21	21	36	21

rapidly decreases IFP to a range of 20–30 mm Hg, enabling collapsed arterioles and capillaries to open. Without additional treatment, HA is replenished, in part by α-SMA(+) myofibroblasts, and intratumoral physical dynamics are restored. Together with a concomitant cytotoxic agent, however, the resultant death of activated PSC leads to the additional loss of collagen I content through decreased synthesis, while also unraveling its architecture, which itself has been implicated in promoting carcinoma invasion and metastasis (Provenzano et al., 2006; Wang et al., 2002), impeding drug delivery (Eikenes et al., 2004; Netti et al., 2000; Ramanujan et al., 2002), and conferring gemcitabine resistance (Dangi-Garimella et al., 2011). Thus, enzymatic degradation of HA removes the central barrier, allowing drugs to breach the previously impenetrable sanctuary of PDA. A subsequent feed-forward mechanism results in depletion of stromal fibroblasts and carcinoma cells, dissolution of the collagen network, and irrevocable remodeling of the tumor microenvironment. Uniform objective responses ensue, at least until cells can evolve secondary mechanisms of resistance. This gap in time represents an unprecedented opportunity for therapeutic advantage. The persistence of patent vessels enables switching sequentially from one chemotherapeutic regimen to another in hopes of prolonging this window of vulnerability. In this context, revisiting the extensive list of previously presumed "ineffective" agents against PDA (Nieto et al., 2008) represents an obvious starting point, even as additional targets within the tumor stroma are identified and explored (Izeradjene and Hingorani, 2007).

In the context of our current findings, two very recent reports of combination regimens to treat advanced PDA are particularly notable for their shared pharmacokinetic features and their improved success over the current standard. One regimen combined gemcitabine with nab-paclitaxel, an albumin-coated formulation of taxol with an extended half-life of >10 hr in the circulation (Von Hoff et al., 2011). A second regimen, FOLFIRINOX, added bolus dosing of two conventional cytotoxic agents onto a base of prolonged (46 hr) continuous infusion of fluorouracil with each treatment cycle (Conroy et al., 2011). In each case, the sustained exposure to cytotoxic therapy may have helped surmount the relative barriers to perfusion imposed by the ECM of PDA.

Finally, the prospect that augmenting blood flow to a lethal carcinoma may increase its ability to seed metastatic deposits gives pause; however, the dramatically decreased metastatic tumor burden in animals treated with combination therapy is reassuring and no doubt contributes to the observed benefit in overall survival. Indeed, that Gemcitabine+PEGPH20 improves survival in animals with advanced and metastatic disease underscores its potential utility for the majority of patients who present with PDA. These findings also reflect the similar physicochemical principles operant in metastases as in the primary tumor; in fact, our molecular characterization of the ECM suggests that the metastatic microenvironment is further enriched in GAGs (including HA) relative to collagen as compared with primary tumors. Understanding the precise mechanism of achieving a decreased metastatic tumor burden has important implications for specific clinical uses of PEGPH20. The decreased metastatic burden may have been achieved by regression of established metastases (which we have observed) and/or decreased seeding of metastases either by killing primary tumor cells or altering their ability to spread. HA has been directly implicated in increasing the metastatic potential of cancer cells (Zhang et al., 1995). However, HA depletion may also inhibit the ability of already seeded cells to establish clinically relevant metastases. In other words, HA may represent a necessary component of the microenvironmental niche in order for a circulating tumor cell or nest of cells to blossom fully into a life-limiting lesion. Thus, there may be additional potential uses for and benefits from a stromal targeting therapy including, for example, as part of an adjuvant regimen. Given that more than two thirds of patients with resected PDA eventually succumb to metastatic disease (Hidalgo, 2010), incorporating an enzymatic agent that degrades HA in the adjuvant setting may extend survival by preventing, or at least delaying, the establishment of a critical metastatic disease burden.

EXPERIMENTAL PROCEDURES

Mouse Strains

All animal studies were approved by the Institutional Animal Care and Use Committee of the Fred Hutchinson Cancer Research Center. *Kras*$^{LSL\text{-}G12D/+}$; *Trp53*$^{LSL\text{-}R172H/+}$;*Cre* (*KPC*) mice have been previously described in detail (Hingorani et al., 2005). *KPC* mice conditionally express endogenous physiologic levels of activated *Kras* and point mutant *Trp53* targeted to progenitor cells of the developing pancreas. The animals spontaneously develop the full spectrum of precursor ductal lesions (pancreatic intraepithelial neoplasias, PanINs) which progress to invasive and metastatic PDA, faithfully mimicking the clinical syndrome, histopathology, and molecular progression of the human disease from inception to invasion and metastasis. A subset of experiments were also performed on *Kras*$^{LSL\text{-}G12D/+}$;*Cre* (*KC*) mice, which similarly develop invasive and metastatic disease along the PanIN-to-PDA progression scheme, albeit with a slower time course than *KPC* mice (Hingorani et al., 2003). *ROSA26*$^{LSL\text{-}EGFP}$ mice (obtained from Jackson Laboratory) contain enhanced green fluorescent protein (EGFP) cDNA sequence flanked by *LoxP* sites knocked-in to the *ROSA26* locus.

Measuring Interstitial Fluid Pressure

Interstitial fluid pressure (IFP) measurements were performed using a Millar Mikro-Tip pressure catheter transducer (SPR-1000, 0.33 mm diameter) with a dynamic pressure range from −50 to 300 mm Hg, possessing a shielded side-mounted sensor. The catheter was connected to PCU-2000 Pressure

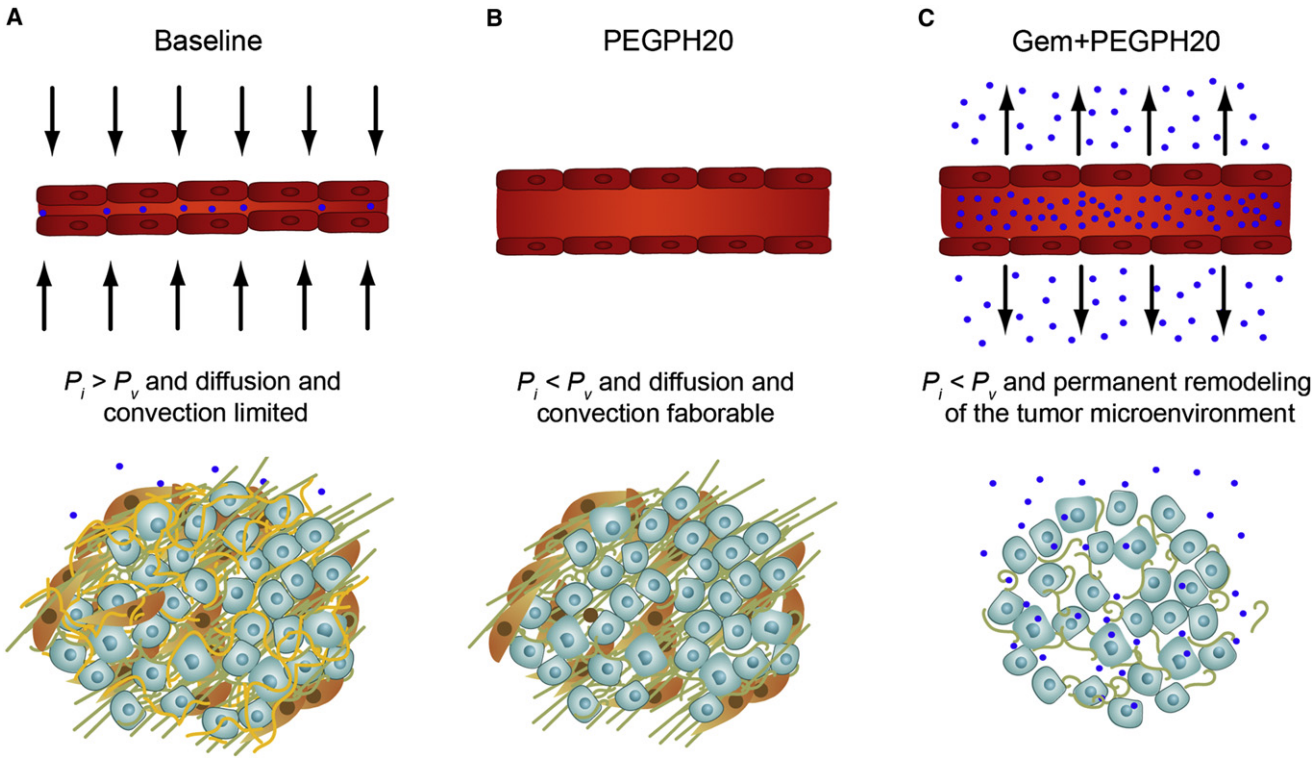

Figure 7. Altering Physicomechanics and Remodeling the Stroma in PDA to Therapeutic Advantage

(A) Intratumoral mechanics in PDA impede diffusion and convection of small molecules.

(B) Enzymatic degradation of stromal HA decreases IFP and relieves physical constraints on small molecule perfusion, which can reconstitute in the absence of additional therapy.

(C) Combined enzymatic and cytotoxic therapy permanently remodels the tumor microenvironment to favor the delivery and distribution of small molecules.

Blue spheres represent chemotherapy molecules, vessels are shown in red, carcinoma cells in light blue, activated PSC in brown, collagen in green, and HA in yellow. P_i, interstitial fluid pressure; P_v, intravascular fluid pressure. See text for details.

Control Unit and an ADInstruments PowerLab data acquisition system (Millar Instruments, Inc.) (Ozerdem and Hargens, 2005; Thompson et al., 2010). Data were recorded and analyzed using LabChart software (Millar Instruments, Inc.). The system was calibrated to 0, 25, and 100 mm Hg prior to each measurement following the manufacturer's recommendations; calibration was reconfirmed after each study. To place the microtip pressure catheter, a 25-gauge needle (~2× the diameter of the probe) was first introduced into the tissue or tumor of interest, and the probe was inserted into the space after needle withdrawal.

Assessment of Vascular Function and Molecular Diffusion

To assess vascular function, 425 μl of biotin-conjugated *Lycopersicon esculentum* lectin (B1175-1mg, Vector Laboratories) was mixed with 75 μl of Streptavidin-AlexaFluor-488 (S32354, Molecular Probes) for whole-tissue MPLSM imaging or with Streptavidin-AlexaFluor-647 (S21375) for analyses of tissue sections following coadministration of doxorubicin (Sigma). Mice were anesthetized by inhalation of isofluorane gas. Five minutes prior to euthanasia, 100 μl of the conjugated lectin was administered into the left ventricle. For coadministration experiments, 20 mg/kg doxorubicin solution was injected immediately after fluorescently conjugated lectin. While under terminal anesthesia, mice were perfused with 4% paraformaldehyde. For histologic analyses, harvested tissues were additionally fixed overnight in 4% paraformaldehyde.

Treatment Schedule and Survival Study

Enrollment of *KPC* mice was based on primary tumor burden and informed by age. Specifically, animals 12–14 weeks old and with a palpable pancreas mass were enrolled. Ultrasound imaging was performed in the initial 11 mice enrolled to confirm the physical examination findings of estimated tumor burden. *KPC* mice were genotyped and then randomized by one investigator (A.E.C.) to receive Gemcitabine+Placebo or Gemcitabine+PEGPH20, which were administered by another investigator (P.P.P.). Objective response was assessed by high-resolution ultrasound performed by a third investigator (C.C.) who was blinded to the treatments administered. The treatment schedule was modeled on the standard clinical management of patients with pancreas cancer (Figure 3A). Gemcitabine was administered intravenously (i.v.) once weekly at 50 mg/kg in a three weeks on/one week off schedule; PEGPH20 (or vehicle) was administered i.v. 24 hr prior to gemcitabine.

Statistical Analyses

Data were tested to determine whether they met the assumption of normality using the Kolmogorov-Smirnov test. Normally distributed two-group data were analyzed using a t test. Multigroup data were analyzed using ANOVA followed with the Newman-Kuels multiple comparison post test. In the instance that two-group data did not conform to normality, the nonparametric Mann-Whitney sum rank test was performed. Kaplan-Meier survival data were analyzed using a log rank test. Metastatic disease burden was analyzed using Fisher's exact test.

SUPPLEMENTAL INFORMATION

Supplemental Information includes six figures, one table, and Supplemental Experimental Procedures and can be found with this article online at doi:10.1016/j.ccr.2012.01.007.

ACKNOWLEDGMENTS

We thank Randi Simmons, Markus Carlson, and Simon Bennett for assistance with animal husbandry and care; Julie Randolph-Habecker and members of FHCRC Experimental Histopathology for assistance with histology and immunohistochemistry; and members of the Hingorani and Olson laboratories for helpful discussions. We thank Shelley Thorsen for expert assistance with figure and manuscript preparation, John Potter for helpful discussions and comments on the manuscript, and Gregory Frost and Michael Shepard for providing PEGPH20 and for helpful discussions. TMA sections were kindly provided by Galen Hostetter and Clifford Whatcott. D.D.V.H. has a consulting agreement with Halozyme Therapeutics. This work was supported by the National Cancer Institute (grants CA161112 and CA114028 to S.R.H., CA152249 to P.P.P. and S.R.H., and CA109552 to D.D.V.H.), the Giles W. and Elise G. Mead Foundation (support to S.R.H.), donated funds from David Jones and Maryanne Tagney-Jones (support to S.R.H.), donated funds from Safeway (support to S.R.H.), and a Jaconette L. Tietze Young Scientist Award (to P.P.P.).

Received: September 30, 2011
Revised: November 26, 2011
Accepted: January 11, 2012
Published: March 19, 2012

REFERENCES

Allison, D.C., Piantadosi, S., Hruban, R.H., Dooley, W.C., Fishman, E.K., Yeo, C.J., Lillemoe, K.D., Pitt, H.A., Lin, P., and Cameron, J.L. (1998). DNA content and other factors associated with ten-year survival after resection of pancreatic carcinoma. J. Surg. Oncol. *67*, 151–159.

Balazs, E.A., and Denlinger, J.L. (1989). Clinical uses of hyaluronan. Ciba Found. Symp. *143*, 265–275, discussion 275–280, 281–265.

Bissell, M.J., and Radisky, D. (2001). Putting tumours in context. Nat. Rev. Cancer *1*, 46–54.

Boucher, Y., and Jain, R.K. (1992). Microvascular pressure is the principal driving force for interstitial hypertension in solid tumors: implications for vascular collapse. Cancer Res. *52*, 5110–5114.

Boucher, Y., Kirkwood, J.M., Opacic, D., Desantis, M., and Jain, R.K. (1991). Interstitial hypertension in superficial metastatic melanomas in humans. Cancer Res. *51*, 6691–6694.

Bouzin, C., and Feron, O. (2007). Targeting tumor stroma and exploiting mature tumor vasculature to improve anti-cancer drug delivery. Drug Resist. Updat. *10*, 109–120.

Brekken, C., Hjelstuen, M.H., Bruland, O.S., and de Lange Davies, C. (2000). Hyaluronidase-induced periodic modulation of the interstitial fluid pressure increases selective antibody uptake in human osteosarcoma xenografts. Anticancer Res. *20* (5B), 3513–3519.

Burris, H.A., 3rd, Moore, M.J., Andersen, J., Green, M.R., Rothenberg, M.L., Modiano, M.R., Cripps, M.C., Portenoy, R.K., Storniolo, A.M., Tarassoff, P., et al. (1997). Improvements in survival and clinical benefit with gemcitabine as first-line therapy for patients with advanced pancreas cancer: a randomized trial. J. Clin. Oncol. *15*, 2403–2413.

Casper, E.S., Green, M.R., Kelsen, D.P., Heelan, R.T., Brown, T.D., Flombaum, C.D., Trochanowski, B., and Tarassoff, P.G. (1994). Phase II trial of gemcitabine (2,2′-difluorodeoxycytidine) in patients with adenocarcinoma of the pancreas. Invest. New Drugs *12*, 29–34.

Conroy, T., Desseigne, F., Ychou, M., Bouché, O., Guimbaud, R., Bécouarn, Y., Adenis, A., Raoul, J.L., Gourgou-Bourgade, S., de la Fouchardière, C., et al; Groupe Tumeurs Digestives of Unicancer; PRODIGE Intergroup. (2011). FOLFIRINOX versus gemcitabine for metastatic pancreatic cancer. N. Engl. J. Med. *364*, 1817–1825.

Curti, B.D., Urba, W.J., Alvord, W.G., Janik, J.E., Smith, J.W., 2nd, Madara, K., and Longo, D.L. (1993). Interstitial pressure of subcutaneous nodules in melanoma and lymphoma patients: changes during treatment. Cancer Res. *53* (10, Suppl), 2204–2207.

Dangi-Garimella, S., Krantz, S.B., Barron, M.R., Shields, M.A., Heiferman, M.J., Grippo, P.J., Bentrem, D.J., and Munshi, H.G. (2011). Three-dimensional collagen I promotes gemcitabine resistance in pancreatic cancer through MT1-MMP-mediated expression of HMGA2. Cancer Res. *71*, 1019–1028.

Eikenes, L., Bruland, O.S., Brekken, C., and Davies, Cde.L. (2004). Collagenase increases the transcapillary pressure gradient and improves the uptake and distribution of monoclonal antibodies in human osteosarcoma xenografts. Cancer Res. *64*, 4768–4773.

Eikenes, L., Tari, M., Tufto, I., Bruland, O.S., and de Lange Davies, C. (2005). Hyaluronidase induces a transcapillary pressure gradient and improves the distribution and uptake of liposomal doxorubicin (Caelyx) in human osteosarcoma xenografts. Br. J. Cancer *93*, 81–88.

Farnell, M.B., Pearson, R.K., Sarr, M.G., DiMagno, E.P., Burgart, L.J., Dahl, T.R., Foster, N., and Sargent, D.J.; Pancreas Cancer Working Group. (2005). A prospective randomized trial comparing standard pancreatoduodenectomy with pancreatoduodenectomy with extended lymphadenectomy in resectable pancreatic head adenocarcinoma. Surgery *138*, 618–628, discussion 628–630.

Heldin, C.H., Rubin, K., Pietras, K., and Ostman, A. (2004). High interstitial fluid pressure: an obstacle in cancer therapy. Nat. Rev. Cancer *4*, 806–813.

Hertel, L.W., Boder, G.B., Kroin, J.S., Rinzel, S.M., Poore, G.A., Todd, G.C., and Grindey, G.B. (1990). Evaluation of the antitumor activity of gemcitabine (2′,2′-difluoro-2′-deoxycytidine). Cancer Res. *50*, 4417–4422.

Hidalgo, M. (2010). Pancreatic cancer. N. Engl. J. Med. *362*, 1605–1617.

Hingorani, S.R., Petricoin, E.F., Maitra, A., Rajapakse, V., King, C., Jacobetz, M.A., Ross, S., Conrads, T.P., Veenstra, T.D., Hitt, B.A., et al. (2003). Preinvasive and invasive ductal pancreatic cancer and its early detection in the mouse. Cancer Cell *4*, 437–450.

Hingorani, S.R., Wang, L., Multani, A.S., Combs, C., Deramaudt, T.B., Hruban, R.H., Rustgi, A.K., Chang, S., and Tuveson, D.A. (2005). Trp53R172H and KrasG12D cooperate to promote chromosomal instability and widely metastatic pancreatic ductal adenocarcinoma in mice. Cancer Cell *7*, 469–483.

Izeradjene, K., and Hingorani, S.R. (2007). Targets, trials, and travails in pancreas cancer. J. Natl. Compr. Canc. Netw. *5*, 1042–1053.

Jacobson, A., Salnikov, A., Lammerts, E., Roswall, P., Sundberg, C., Heldin, P., Rubin, K., and Heldin, N.E. (2003). Hyaluronan content in experimental carcinoma is not correlated to interstitial fluid pressure. Biochem. Biophys. Res. Commun. *305*, 1017–1023.

Jain, R.K. (1987). Transport of molecules across tumor vasculature. Cancer Metastasis Rev. *6*, 559–593.

Jain, R.K. (1990). Vascular and interstitial barriers to delivery of therapeutic agents in tumors. Cancer Metastasis Rev. *9*, 253–266.

Janssen, B.J., Leenders, P.J., and Smits, J.F. (2000). Short-term and long-term blood pressure and heart rate variability in the mouse. Am. J. Physiol. Regul. Integr. Comp. Physiol. *278*, R215–R225.

Jemal, A., Siegel, R., Xu, J., and Ward, E. (2010). Cancer statistics, 2010. CA Cancer J. Clin. *60*, 277–300.

Kedem, O., and Katchalsky, A. (1958). Thermodynamic analysis of the permeability of biological membranes to non-electrolytes. Biochim. Biophys. Acta *27*, 229–246.

Kedem, O., and Katchalsky, A. (1961). A physical interpretation of the phenomenological coefficients of membrane permeability. J. Gen. Physiol. *45*, 143–179.

Less, J.R., Posner, M.C., Boucher, Y., Borochovitz, D., Wolmark, N., and Jain, R.K. (1992). Interstitial hypertension in human breast and colorectal tumors. Cancer Res. *52*, 6371–6374.

Mattson, D.L. (1998). Long-term measurement of arterial blood pressure in conscious mice. Am. J. Physiol. *274*, R564–R570.

Michel, C.C. (1984). Fluid movements through capillary walls. In Handbook of Physiology, Section 2, Vol. IV, Microcirculation, E.M. Renkin and C.C. Michel, eds. (Washington, D.C: American Physiological Society), pp. 375–409.

Moore, M.J., Goldstein, D., Hamm, J., Figer, A., Hecht, J.R., Gallinger, S., Au, H.J., Murawa, P., Walde, D., Wolff, R.A., et al; National Cancer Institute of Canada Clinical Trials Group. (2007). Erlotinib plus gemcitabine compared with gemcitabine alone in patients with advanced pancreatic cancer: a phase

III trial of the National Cancer Institute of Canada Clinical Trials Group. J. Clin. Oncol. *25*, 1960–1966.

Netti, P.A., Hamberg, L.M., Babich, J.W., Kierstead, D., Graham, W., Hunter, G.J., Wolf, G.L., Fischman, A., Boucher, Y., and Jain, R.K. (1999). Enhancement of fluid filtration across tumor vessels: implication for delivery of macromolecules. Proc. Natl. Acad. Sci. USA *96*, 3137–3142.

Netti, P.A., Berk, D.A., Swartz, M.A., Grodzinsky, A.J., and Jain, R.K. (2000). Role of extracellular matrix assembly in interstitial transport in solid tumors. Cancer Res. *60*, 2497–2503.

Nieto, J., Grossbard, M.L., and Kozuch, P. (2008). Metastatic pancreatic cancer 2008: is the glass less empty? Oncologist *13*, 562–576.

Oettle, H., Post, S., Neuhaus, P., Gellert, K., Langrehr, J., Ridwelski, K., Schramm, H., Fahlke, J., Zuelke, C., Burkart, C., et al. (2007). Adjuvant chemotherapy with gemcitabine vs observation in patients undergoing curative-intent resection of pancreatic cancer: a randomized controlled trial. JAMA *297*, 267–277.

Ogston, A.G., and Michel, C.C. (1978). General descriptions of passive transport of neutral solute and solvent through membranes. Prog. Biophys. Mol. Biol. *34*, 197–217.

Olive, K.P., Jacobetz, M.A., Davidson, C.J., Gopinathan, A., McIntyre, D., Honess, D., Madhu, B., Goldgraben, M.A., Caldwell, M.E., Allard, D., et al. (2009). Inhibition of Hedgehog signaling enhances delivery of chemotherapy in a mouse model of pancreatic cancer. Science *324*, 1457–1461.

Ozerdem, U., and Hargens, A.R. (2005). A simple method for measuring interstitial fluid pressure in cancer tissues. Microvasc. Res. *70*, 116–120.

Provenzano, P.P., Eliceiri, K.W., Campbell, J.M., Inman, D.R., White, J.G., and Keely, P.J. (2006). Collagen reorganization at the tumor-stromal interface facilitates local invasion. BMC Med. *4*, 38.

Ramanujan, S., Pluen, A., McKee, T.D., Brown, E.B., Boucher, Y., and Jain, R.K. (2002). Diffusion and convection in collagen gels: implications for transport in the tumor interstitium. Biophys. J. *83*, 1650–1660.

Reed, R.K., Rubin, K., Wiig, H., and Rodt, S.A. (1992). Blockade of beta 1-integrins in skin causes edema through lowering of interstitial fluid pressure. Circ. Res. *71*, 978–983.

Schultz, R.M., Merriman, R.L., Toth, J.E., Zimmermann, J.E., Hertel, L.W., Andis, S.L., Dudley, D.E., Rutherford, P.G., Tanzer, L.R., and Grindey, G.B. (1993). Evaluation of new anticancer agents against the MIA PaCa-2 and PANC-1 human pancreatic carcinoma xenografts. Oncol. Res. *5*, 223–228.

Sherwood, L. (1997). Human Physiology from Cells to Systems, Third Edition (Florence, KY: Wadsworth Publishing Company).

Starling, E.H. (1896). On the absorption of fluids from the connective tissue spaces. J. Physiol. *19*, 312–326.

Staverman, A.J. (1952). Non-equilibrium thermodynamics of membrane processes. Trans. Faraday Soc. *48*, 176–185. 10.1039/TF9524800176.

Tempero, M., Plunkett, W., Ruiz Van Haperen, V., Hainsworth, J., Hochster, H., Lenzi, R., and Abbruzzese, J. (2003). Randomized phase II comparison of dose-intense gemcitabine: thirty-minute infusion and fixed dose rate infusion in patients with pancreatic adenocarcinoma. J. Clin. Oncol. *21*, 3402–3408.

Thompson, C.B., Shepard, H.M., O'Connor, P.M., Kadhim, S., Jiang, P., Osgood, R.J., Bookbinder, L.H., Li, X., Sugarman, B.J., Connor, R.J., et al. (2010). Enzymatic depletion of tumor hyaluronan induces antitumor responses in preclinical animal models. Mol. Cancer Ther. *9*, 3052–3064.

Toole, B.P. (2004). Hyaluronan: from extracellular glue to pericellular cue. Nat. Rev. Cancer *4*, 528–539.

Toole, B.P., and Slomiany, M.G. (2008). Hyaluronan: a constitutive regulator of chemoresistance and malignancy in cancer cells. Semin. Cancer Biol. *18*, 244–250.

Trédan, O., Galmarini, C.M., Patel, K., and Tannock, I.F. (2007). Drug resistance and the solid tumor microenvironment. J. Natl. Cancer Inst. *99*, 1441–1454.

Ueno, H., Kiyosawa, K., and Kaniwa, N. (2007). Pharmacogenomics of gemcitabine: can genetic studies lead to tailor-made therapy? Br. J. Cancer *97*, 145–151.

Von Hoff, D.D., Ramanathan, R.K., Borad, M.J., Laheru, D.A., Smith, L.S., Wood, T.E., Korn, R.L., Desai, N., Trieu, V., Iglesias, J.L., et al. (2011). Gemcitabine plus nab-paclitaxel is an active regimen in patients with advanced pancreatic cancer: a phase I/II trial. J. Clin. Oncol. *29*, 4548–4554.

Wang, W., Wyckoff, J.B., Frohlich, V.C., Oleynikov, Y., Hüttelmaier, S., Zavadil, J., Cermak, L., Bottinger, E.P., Singer, R.H., White, J.G., et al. (2002). Single cell behavior in metastatic primary mammary tumors correlated with gene expression patterns revealed by molecular profiling. Cancer Res. *62*, 6278–6288.

Zhang, L., Underhill, C.B., and Chen, L. (1995). Hyaluronan on the surface of tumor cells is correlated with metastatic behavior. Cancer Res. *55*, 428–433.